

Asymmetric Absorption Profiles of Ly α and Ly β in Damped Lyman Alpha Systems

Hee-Won Lee

Department of Astronomy and Space Science, Sejong University, Seoul, 143-747, Korea
hwlee@sejong.ac.kr

ABSTRACT

Damped Ly α systems (DLAs) observed in the quasar spectra are characterized by a high neutral hydrogen column density $N_{HI} > 2 \times 10^{20} \text{ cm}^{-2}$. The absorption wing profiles are often fitted using the Voigt function due to the fact that the scattering cross section near resonant line center is approximately described by the Lorentzian function. Since a hydrogen atom has infinitely many p states that participate in the electric dipole interaction, the cross section starts to deviate from the Lorentzian in an asymmetric way in the line wing regions. We investigate this asymmetry in the absorption line profiles around Ly α and Ly β as a function of the neutral hydrogen column density N_{HI} . In terms of $\Delta\lambda \equiv \lambda - \lambda_\alpha$ we expand the Kramers-Heisenberg formula around Ly α to find $\sigma(\lambda) \simeq (0.5f_{12})^2\sigma_T(\Delta\lambda/\lambda_\alpha)^{-2}[1 + 3.792(\Delta\lambda/\lambda_\alpha)]$, where f_{12} and σ_T are the oscillator strength of Ly α and the Thomson scattering cross section, respectively. In terms of $\Delta\lambda_2 \equiv \lambda - \lambda_\beta$ in the vicinity of Ly β , the total scattering cross section, given as the sum of cross sections for Rayleigh and Raman scattering, is shown to be $\sigma(\lambda) \simeq \sigma_T(0.5f_{13})^2(1 + R_0)(\Delta\lambda_2/\lambda_\beta)^{-2}[1 - 24.68(\Delta\lambda_2/\lambda_\beta)]$ with f_{13} and the factor $R_0 = 0.1342$ being the oscillator strength for Ly β and the ratio of Raman cross section to Rayleigh cross section, respectively. A redward asymmetry develops around Ly α whereas a blue asymmetry is obtained for Ly β . The absorption center shifts are found to be almost proportional to the neutral hydrogen column density.

1. Introduction

Hydrogen is the most abundant element in the universe and therefore is an important probe for the physical conditions of intergalactic medium throughout the observable universe.

High resolution spectroscopy of quasars shows a large number of absorption lines blueward of Ly α mostly due to neutral hydrogen components in intergalactic medium intervening along the line of sight. These quasar absorption systems due to hydrogen are classified according to the H I column densities. Quasar absorption systems with a neutral column density not exceeding $N_{HI} \simeq 10^{17} \text{ cm}^{-2}$ constitute the Ly α forest which is attributed to the residual hydrogen atoms contained in intergalactic filamentary structures that are highly ionized (e.g. Rauch 1998, Meiksin 2009, Kim et al. 2011). The absorption systems associated with a neutral hydrogen column density in excess of $N_{HI} = 10^{20.3} \text{ cm}^{-2}$ are called the damped Lyman alpha systems (DLAs), which are distinguished from other quasar absorption systems in that they are dominantly neutral (e.g. Wolfe et al. 1986, 2005).

A catalogue of 322 DLAs was provided by Curran et al. (2002), and recently 721 DLAs are listed from the Sloan Digital Sky Survey Data Release 7 (Khare et al. 2012). The exact nature of the DLAs is still controversial, but they are believed to dominate the neutral gas content in the universe, providing raw material for star formation during most of the time from the reionization era to the present (e.g. Wolfe et al. 2005, Prochaska, Herbert-Fort & Wolfe 2005). DLAs are also important to trace the chemical evolution of the universe by carefully measuring the metal abundance as a function of redshift (e.g. Calura, Matteucci & Vladilo 2003, Rafelski et al. 2012). Accurate atomic physics for Ly α is essential to obtain a reliable estimate of metallicity of a DLA.

Recently, Kulkarni et al. (2012) reported a discovery of "super-damped" Lyman-alpha absorber at $z_{abs} = 2.2068$ toward the QSO Q1135-0010. Their profile fit to the DLA showed a high neutral hydrogen column density of $N_{HI} = 10^{22.05} \text{ cm}^{-2}$. A little higher column density of $N_{HI} = 10^{22.10} \text{ cm}^{-2}$ was reported for the same object by Noterdaeme et al. (2012), who also suggested a significant star formation rate of $25 M_{\odot} \text{ yr}^{-1}$ based on the strength of H α .

Damped Ly α absorption profiles are analyzed using the Voigt function which is defined as a convolution of a Lorentzian function with a Gaussian function (e.g. Rybicki & Lightman 1979). When N_{HI} is very large, the absorption at the core part is almost complete. Contributing only to the core part of the Voigt function, the Gaussian function does not play an important role in the analysis of high column density systems. In the wing part the Voigt function coincides with the Lorentzian, and in this case the damping term in the denominator of the Lorentzian is quite negligible. Therefore, the wing profile is essentially proportional to $\Delta\lambda^{-2}$, where $\Delta\lambda = \lambda - \lambda_{\alpha}$ is the difference in wavelength from the Ly α line center wavelength $\lambda_{\alpha} = 1215.671 \text{ \AA}$.

The Lorentzian function, invoked to describe the wing parts of the absorption profile, is obtained when the scattering atom is regarded as a two-level atom. Instead of being a two-level system, the hydrogen atom has infinitely many energy levels, and therefore the

scattering cross section is expected to deviate from the Lorentzian function that is symmetric with respect to the line center wavelength. Peebles (1993) discussed the resonance line shape that deviates from the simple Lorentzian and mentioned the marginal possibility of detecting this deviation in the absorption line profiles of DLA systems (e.g. Peebles 1993, p. 573). The formula for the scattering cross section he introduced is derived in a heuristic way to illustrate the behavior of the Lorentzian profile near line resonance and the classical ω^4 -dependence in the low energy regime. However, this formula is inaccurate because it fails to include the contributions from the infinitely many p states that participate in the electric dipole interaction.

The exact scattering cross section is computed by summing all the probability amplitudes contributed from the infinitely many bound and free p states. The result is summarized in the Kramers-Heisenberg formula (e.g. Bethe & Salpeter 1967, Sakurai 1967). An expansion of the Kramers-Heisenberg formula around Ly α in frequency space was given by Lee (2003), in which the redward asymmetry of the scattering cross section around Ly α was briefly illustrated. However, spectroscopy is often presented in wavelength space rather than in frequency space so that it will also be useful to express the Kramers-Heisenberg formula in wavelength space. In this paper, we present the same expansion in wavelength space and quantify the redward shift of the center wavelength as a function of N_{HI} . In addition, we also expand the Kramers-Heisenberg formula in the vicinity of Ly β in order to investigate the asymmetry around Ly β .

In the case of Ly β , there is an additional scattering channel, which results from radiative de-excitation into the $2s$ state re-emitting an H α line photon. This inelastic or Raman scattering branch is proposed to be important in the formation of broad H α wings observed in young planetary nebulae and symbiotic stars (e.g. Isliker, Nussbaumer & Vogel 1989, Lee 2000, Schmid 1989). In this paper, we show that the cross section around Ly β is asymmetric blueward, which is in high contrast with the behavior around Ly α . A brief discussion on the observational consequences is presented.

2. Calculation

2.1. Scattering cross section around Ly α in wavelength space

The scattering cross section is given by the Kramers-Heisenberg formula that is obtained from a second-order time dependent perturbation theory (e.g. Sakurai 1967, Merzbacher 1970). In terms of the matrix elements of the dipole operator, the Kramers-Heisenberg

formula can be written as

$$\begin{aligned} \frac{d\sigma}{d\Omega} = & \frac{r_0^2 m_e^2}{\hbar^2} \left| \sum_I \omega \omega_{I1} \left(\frac{(\mathbf{r} \cdot \mathbf{e}^{(\alpha')})_{1I} (\mathbf{r} \cdot \mathbf{e}^{(\alpha)})_{I1}}{\omega_{I1} - \omega} \right. \right. \\ & \left. \left. - \frac{(\mathbf{r} \cdot \mathbf{e}^{(\alpha)})_{1I} (\mathbf{r} \cdot \mathbf{e}^{(\alpha')})_{I1}}{\omega_{I1} + \omega} \right) \right|^2, \end{aligned} \quad (1)$$

where m_e is the electron mass and $r_0 = e^2/m_e c^2$ is the classical electron radius. The polarization vectors of incident and scattered radiation are denoted by $\mathbf{e}^{(\alpha)}$ and $\mathbf{e}^{(\alpha')}$, respectively. Here, ω_{I1} is the angular frequency between the intermediate state I and the ground $1s$ state. The intermediate state I that participates in the electric dipole interaction of Lyman photons consists of bound np states and free $n'p$ states. In the atomic units adopted in this work, the bound np state has the energy eigenvalue $E_n = -1/(2n^2)$ and correspondingly $\omega_{I1} = \omega_{n1} = (1 - n^{-2})/2$. Similarly, for the $n'p$ state, $E_{n'} = 1/(2n'^2)$ and $\omega_{I1} = \omega_{n'1} = (1 + n'^{-2})/2$. The term denoted by $(\mathbf{r} \cdot \mathbf{e}^{(\alpha)})_{I1}$ represents the matrix element of the position operator between the intermediate state I and the ground $1s$ state.

Being a two-body system, the hydrogen atom admits analytically closed expressions of the wavefunctions, which enables one to compute explicitly the matrix elements of the dipole operator in terms of the confluent hypergeometric function. A typical matrix element $(\mathbf{r} \cdot \mathbf{e}^{(\alpha)})_{I1}$ for an intermediate state with $I = |np, m\rangle$ is explicitly written as

$$(\mathbf{r} \cdot \mathbf{e}^{(\alpha)})_{I1} = \int_0^{2\pi} \int_0^\pi \int_0^\infty [R_{nl}(r) Y_l^m(\theta, \phi)]^* (\mathbf{r} \cdot \mathbf{e}^{(\alpha)}) R_{10}(r) Y_0^0(\theta, \phi) r^2 dr \sin\theta d\theta d\phi, \quad (2)$$

where $Y_l^m(\theta, \phi)$ is a spherical harmonic function and $R_{nl}(r)$ is the radial wavefunction given by an associated Laguerre function. The angular integration followed by summing over magnetic substates $m = \pm 1, 0$ of each np state and averaging over polarization states of incident and outgoing radiation results in a numerical factor of $\frac{8\pi}{3}$, which is discussed in more detail in Appendix A.

The radial matrix elements of the dipole operators $\langle r \rangle_{n1}$ and $\langle r \rangle_{n',1}$ are readily found in many textbooks on quantum mechanics (e.g. Berestetski, Lifshitz & Pitaevskii 1971, Bethe & Salpeter 1967). The radial matrix elements for the bound np states are given by

$$\langle r \rangle_{1n} = \langle 1s | r | np \rangle = \left[\frac{2^8 n^7 (n-1)^{2n-5}}{(n+1)^{2n+5}} \right]^{\frac{1}{2}} a_B, \quad (3)$$

where $a_B = \hbar^2/m_e e^2 = 0.5292 \text{ \AA}$ is the Bohr radius. For the continuum $n'p$ states, the corresponding values are given by

$$\langle r \rangle_{1n'} = \langle 1s | r | n'p \rangle = \left[\frac{2^8 (n')^7 \exp[-4n' \tan^{-1}(1/n')]}{[(n')^2 + 1]^5 [1 - \exp(-2\pi n')]} \right]^{\frac{1}{2}} a_B, \quad (4)$$

which is obtained through analytic continuation into the complex plane (Bethe & Salpeter 1967, Saslow & Mills 1969).

Lee (2003) provided the expansion of the Kramers-Heisenberg formula for Rayleigh scattering in the vicinity of Ly α in terms of $\Delta\omega = \omega - \omega_{21}$. The result is summarized as

$$\begin{aligned} \sigma(\omega) = & \sigma_T \left(\frac{f_{12}}{2} \right)^2 \left(\frac{\omega_{21}}{\Delta\omega} \right)^2 \left| 1 + a_1 \left(\frac{\Delta\omega}{\omega_{21}} \right) \right. \\ & \left. + a_2 \left(\frac{\Delta\omega}{\omega_{21}} \right)^2 + \dots \right|^2, \end{aligned} \quad (5)$$

where $\sigma_T = 8\pi r_0^2/3 = 0.6652 \times 10^{-24} \text{ cm}^2$ is the Thomson scattering cross section and $f_{12} = 0.4162$ is the oscillator strength for the Ly α transition. The coefficients a_k were numerically computed by Lee (2003), who gave

$$a_1 = -8.961 \times 10^{-1}, \quad a_2 = -1.222 \times 10^1. \quad (6)$$

In Table 1, we show these coefficients up to a_5 .

Up to the first order of $\Delta\omega/\omega_{12}$ the scattering cross section can be expressed as

$$\begin{aligned} \sigma(\omega) & \simeq \sigma_T \left(\frac{f_{12}}{2} \right)^2 \left(\frac{\omega_{12}}{\Delta\omega} \right)^2 \left(1 + 2a_1 \frac{\Delta\omega}{\omega_{21}} \right) \\ & = \sigma_\alpha \left(\frac{\omega_{12}}{\Delta\omega} \right)^2 \left(1 - 1.792 \frac{\Delta\omega}{\omega_{21}} \right). \end{aligned} \quad (7)$$

Here, we introduce the characteristic cross section σ_α for Ly α defined as $\sigma_\alpha \equiv \sigma_T (f_{12}/2)^2 = 2.880 \times 10^{-26} \text{ cm}^2$. The coefficient a_1 , being less than zero, is responsible for the redward asymmetric deviation of the scattering cross section in frequency space.

Astronomical spectroscopy is often presented in wavelength space, which makes it necessary to express the scattering cross section in terms of $\Delta\lambda = \lambda - \lambda_\alpha$, the difference in wavelength from the Ly α line center. From the following relation

$$\frac{\Delta\omega}{\omega_\alpha} = -\frac{\Delta\lambda}{\lambda} = \sum_{n=1}^{\infty} \left(-\frac{\Delta\lambda}{\lambda_\alpha} \right)^n, \quad (8)$$

we may notice that expansion in wavelength space will yield different coefficients from those obtained in expansion in frequency space. Substituting Eq. (8) into Eq. (7), we obtain

$$\sigma(\lambda) \simeq \sigma_T \left(\frac{f_{12}}{2} \right)^2 \left(\frac{\lambda_\alpha}{\Delta\lambda} \right)^2 \left[1 + 2(1 - a_1) \left(\frac{\Delta\lambda}{\lambda_\alpha} \right) \right]$$

$$\begin{aligned}
& + (1 - 2a_1 + 2a_2 - a_1^2) \left(\frac{\Delta\lambda}{\lambda_\alpha} \right)^2 \\
& - 2(a_3 + a_1 a_2) \left[\left(\frac{\Delta\lambda}{\lambda_\alpha} \right)^3 + \dots \right] \\
& = \sigma_\alpha \left(\frac{\lambda_\alpha}{\Delta\lambda} \right)^2 \left[1 + 3.792 \left(\frac{\Delta\lambda}{\lambda_\alpha} \right) \right. \\
& \left. - 20.84 \left(\frac{\Delta\lambda}{\lambda_\alpha} \right)^2 + 83.14 \left(\frac{\Delta\lambda}{\lambda_\alpha} \right)^3 + \dots \right]. \tag{9}
\end{aligned}$$

Thus, up to first order, we have

$$\sigma(\lambda) \simeq \sigma_\alpha \left(\frac{\lambda_\alpha}{\Delta\lambda} \right)^2 \left[1 + 3.792 \left(\frac{\Delta\lambda}{\lambda_\alpha} \right) \right], \tag{10}$$

from which it is found that the coefficient 3.792 is significantly different from the coefficient -1.792 in frequency space.

The red asymmetry in the Ly α scattering cross section can be explained by noting the denominator $\omega_{n1} - \omega$ in Eq. (1), where the dominant contribution comes from $n = 2$. The contributions from all the excited states with $n > 2$ interfere positively with the dominant contribution from $n = 2$ for photons on the red side whereas the interference is negative for photons on the blue side. Therefore the red wing is strengthened relative to the pure Lorentzian profile by the positive interference of scattering from all other levels.

2.2. Rayleigh scattering cross section around Ly β

In a similar way, we define the difference in frequency from Ly β by

$$\Delta\omega_2 \equiv \omega - \omega_{31}, \tag{11}$$

and expand the Kramers-Heisenberg formula in terms of $\Delta\omega_2/\omega_{31}$. We note that the terms appearing in the Kramers-Heisenberg formula include

$$\frac{\omega\omega_{31}}{\omega_{31} - \omega} = -\omega_{31} \left(1 + \frac{\omega_{31}}{\Delta\omega_2} \right), \tag{12}$$

and

$$\frac{\omega}{\omega_{n1} - \omega} = \frac{\omega_{31}}{\omega_{n1} - \omega_{31}} \left[1 + \frac{\omega_{n1}}{\omega_{31}} \sum_{k=1}^{\infty} \left(\frac{\Delta\omega_2}{\omega_{n1} - \omega_{31}} \right)^k \right]. \tag{13}$$

For $n \geq 2$, the second term in the summation in Eq. (1) can be written as

$$\frac{\omega}{\omega_{n1} + \omega} = \frac{\omega_{31}}{\omega_{n1} + \omega_{31}} \left[1 - \frac{\omega_{n1}}{\omega_{31}} \sum_{k=1}^{\infty} \left(\frac{-\Delta\omega_2}{\omega_{n1} + \omega_{31}} \right)^k \right]. \quad (14)$$

Similar expressions for the continuum states are obtained in a straightforward manner.

We expand the Kramers-Heisenberg formula in frequency space for Rayleigh scattering near $Ly\beta$, which is written as

$$\begin{aligned} \sigma^{Ray}(\omega) &= \frac{\sigma_T}{9} \left(\frac{\omega_{31}}{\Delta\omega_2} \right)^2 \left| \omega_{31} < r >_{13}^2 + \omega_{31} < r >_{13}^2 \left(\frac{\Delta\omega_2}{\omega_{31}} \right) \right. \\ &- \sum_{n \neq 3} \frac{\Delta\omega_2 \omega_{n1}}{\omega_{n1} - \omega_{31}} \left[1 + \frac{\omega_{n1}}{\omega_{31}} \sum_{k=1}^{\infty} \left(\frac{\Delta\omega_2}{\omega_{n1} - \omega_{31}} \right)^k \right] < r >_{n1}^2 \\ &+ \sum_{n \neq 3} \frac{\Delta\omega_2 \omega_{n1}}{\omega_{n1} + \omega_{31}} \left[1 - \frac{\omega_{n1}}{\omega_{31}} \sum_{k=1}^{\infty} \left(\frac{-\Delta\omega_2}{\omega_{n1} + \omega_{31}} \right)^k \right] < r >_{n1}^2 \\ &- \int_0^{\infty} dn' \frac{\Delta\omega_2 \omega_{n'1}}{\omega_{n'1} - \omega_{31}} \left[1 + \frac{\omega_{n'1}}{\omega_{31}} \sum_{k=1}^{\infty} \left(\frac{\Delta\omega_2}{\omega_{n'1} - \omega_{31}} \right)^k \right] < r >_{n'1}^2 \\ &+ \left. \int_0^{\infty} dn' \frac{\Delta\omega_2 \omega_{n'1}}{\omega_{n'1} + \omega_{31}} \left[1 - \frac{\omega_{n'1}}{\omega_{31}} \sum_{k=1}^{\infty} \left(\frac{-\Delta\omega_2}{\omega_{n'1} + \omega_{31}} \right)^k \right] < r >_{n'1}^2 \right|^2. \quad (15) \end{aligned}$$

Here, angular integration has been performed and the atomic unit system is adopted, in which the Bohr radius $a_B = 1$.

An algebraic rearrangement of Eq. (15) can be made to express $\sigma^{Ray}(\omega)$ as

$$\begin{aligned} \sigma^{Ray}(\omega) &= \sigma_T \left(\frac{\omega_{31}}{\Delta\omega_2} \right)^2 \left| B_0 + B_1 \left(\frac{\Delta\omega_2}{\omega_{31}} \right) \right. \\ &\quad \left. + B_2 \left(\frac{\Delta\omega_2}{\omega_{31}} \right)^2 + \dots \right|^2. \quad (16) \end{aligned}$$

The coefficients B_0 and B_1 are determined through following relations;

$$\begin{aligned} B_0 &= \frac{\omega_{31}}{3} < r >_{13}^2 = f_{13}/2 = 0.03955 \\ B_1 &= \frac{1}{2} \omega_{31} < r >_{13}^2 - \frac{2}{3} \sum_{n \neq 3} \frac{\omega_{31}^2 \omega_{n1}}{\omega_{n1}^2 - \omega_{31}^2} < r >_{n1}^2 \\ &- \frac{2}{3} \int_0^{\infty} dn' \frac{\omega_{31}^2 \omega_{n'1}}{\omega_{n'1}^2 - \omega_{31}^2} < r >_{n'1}^2 = 0.6414, \quad (17) \end{aligned}$$

where $f_{13} = 0.07910$ is the oscillator strength for the Ly β transition. The coefficients B_k for $k \geq 2$ are given as

$$\begin{aligned}
 B_k &= \left(\frac{-1}{2}\right)^k \frac{\omega_{31}}{3} \langle r \rangle_{13}^2 \\
 &- \frac{1}{3} \sum_{n \neq 3}^{\infty} \frac{\omega_{n1}^2}{\omega_{31}} \left[\left(\frac{\omega_{31}}{\omega_{n1} - \omega_{31}}\right)^k - \left(\frac{-\omega_{31}}{\omega_{n1} + \omega_{31}}\right)^k \right] \langle r \rangle_{n1}^2 \\
 &- \frac{1}{3} \int_0^{\infty} dn' \frac{\omega_{n'1}^2}{\omega_{31}} \left[\left(\frac{\omega_{31}}{\omega_{n'1} - \omega_{31}}\right)^k - \left(\frac{-\omega_{31}}{\omega_{n'1} + \omega_{31}}\right)^k \right] \langle r \rangle_{n'1}^2. \tag{18}
 \end{aligned}$$

The numerical values of the coefficients up to $k = 5$ are computed as follows;

$$\begin{aligned}
 b_1 &= B_1/B_0 = 1.621 \times 10^1 \\
 b_2 &= B_2/B_0 = -4.299 \times 10^2 \\
 b_3 &= B_3/B_0 = -2.176 \times 10^3 \\
 b_4 &= B_4/B_0 = -6.005 \times 10^4 \\
 b_5 &= B_5/B_0 = -8.414 \times 10^5. \tag{19}
 \end{aligned}$$

In particular, the coefficient b_1 is positive due to the predominant contribution from the $2p$ state.

Therefore, up to the first order approximation in $\Delta\omega_2/\omega_{31}$, the Rayleigh scattering cross section around Ly β is given by

$$\begin{aligned}
 \sigma^{Ray}(\omega) &\simeq \sigma_T \left(\frac{f_{13}}{2}\right)^2 \left(\frac{\omega_{13}}{\Delta\omega_2}\right)^2 \left(1 + 2b_1 \frac{\Delta\omega_2}{\omega_{31}}\right) \\
 &\simeq \sigma_T \left(\frac{f_{13}}{2}\right)^2 \left(\frac{\omega_{13}}{\Delta\omega_2}\right)^2 \left(1 + 32.42 \frac{\Delta\omega_2}{\omega_{31}}\right). \tag{20}
 \end{aligned}$$

In wavelength space, the Rayleigh scattering cross section in the vicinity of Ly β with the line center $\lambda_\beta = 1025.722 \text{ \AA}$ can be expanded as

$$\begin{aligned}
 \sigma^{Ray}(\lambda) &\simeq \sigma_T \left(\frac{f_{13}}{2}\right)^2 \left(\frac{\lambda_\beta}{\Delta\lambda_2}\right)^2 \left[1 + 2(1 - b_1) \left(\frac{\Delta\lambda_2}{\lambda_\beta}\right) \right. \\
 &+ (1 - 2b_1 + 2b_2 - b_1^2) \left(\frac{\Delta\lambda_2}{\lambda_\beta}\right)^2 \\
 &\left. - 2(b_3 + b_1b_2) \left(\frac{\Delta\lambda_2}{\lambda_\beta}\right)^3 + \dots \right]
 \end{aligned}$$

$$\begin{aligned}
 &= \sigma_T \left(\frac{f_{13}}{2} \right)^2 \left(\frac{\lambda_\beta}{\Delta\lambda_2} \right)^2 \left[1 - 31.64 \left(\frac{\Delta\lambda_2}{\lambda_\beta} \right) \right. \\
 &\quad \left. - 5.970 \times 10^2 \left(\frac{\Delta\lambda_2}{\lambda_\beta} \right)^2 + 1.792 \times 10^4 \left(\frac{\Delta\lambda_2}{\lambda_\beta} \right)^3 \dots \right], \quad (21)
 \end{aligned}$$

where $\Delta\lambda_2 \equiv \lambda - \lambda_\beta$ is the wavelength deviation from the Ly β center.

The negative value of the coefficient $2(1 - b_1)$ implies that the Rayleigh scattering cross section near Ly β is asymmetric to the blue of Ly β , which is in high contrast with the behavior around Ly α . In the case of Ly β , the main contributor to the Kramers-Heisenberg formula is the $3p$ state and the residual contribution comes from the $2p$ state and all the p states lying higher than the $3p$ state. The contribution to $\sigma(\lambda)$ of a given np or $n'p$ state is measured roughly by the oscillator strength inversely weighted by the energy difference from Ly β . Therefore, the contribution of the $2p$ state is more important than that from all the p states lying higher than the $3p$ state. Hence, in the case of Ly β , the $n = 2$ contribution has lower frequency and the interference with the principal $n = 3$ scattering contribution is negative on the red side and positive on the blue side, which explains the blue asymmetric scattering cross section.

2.3. Raman scattering cross section around Ly β

Interaction with a hydrogen atom of electromagnetic radiation around Ly β has another channel, which is inelastic or Raman scattering. The scattering hydrogen atom de-excites into the $2s$ state re-emitting an H α photon into another line of sight, which provides an important contribution to the absorption profile around Ly β . The astrophysical importance of Raman scattering can be appreciated in the emission features at 6830 Å and 7088 Å that appear in the spectra of about a half of symbiotic stars. These are formed through Raman conversion of the resonance doublet O VI $\lambda\lambda$ 1032, 1038 (Schmid 1989, Nussbaumer, Schmid & Vogel 1989). Another example of Raman scattering by atomic hydrogen is provided by far UV He II emission lines in symbiotic stars and young planetary nebulae (e.g. Birriel 2004, Lee et al. 2006, Lee 2012). It has also been proposed that broad H α wings often found in planetary nebulae and symbiotic stars are formed through Raman scattering of far UV continuum around Ly β (e.g. Lee 2000, Arrieta & Torres-Peimbert 2003).

As is illustrated in Sakurai (1967), the term corresponding to the 'seagull graph' is absent in the Kramers-Heisenberg formula for the case of Raman scattering. This difference allows an alternate expression of the Kramers-Heisenberg formula given in terms of the matrix elements of the momentum operator (see also Saslow & Mills 1969, Lee & Lee 1997). In a manner analogous to what is illustrated in Appendix A, taking angular integrations,

summing over magnetic substates and averaging over polarizations of incident and outgoing radiation, we arrive at an explicit expression of the Raman cross section given by

$$\begin{aligned} \sigma^{Ram}(\omega) &= \frac{\sigma_T}{9} \left(\frac{\omega'}{\omega} \right) \left| \sum_{n=3}^{\infty} \langle p \rangle_{n1} \langle p \rangle_{n2} \left(\frac{1}{\omega_{n1} - \omega} + \frac{1}{\omega_{n1} + \omega'} \right) \right. \\ &\quad \left. + \int_0^{\infty} dn' \langle p \rangle_{n'1} \langle p \rangle_{n'2} \left(\frac{1}{\omega_{n'1} - \omega} + \frac{1}{\omega_{n'1} + \omega'} \right) \right|^2. \end{aligned} \quad (22)$$

Here $\omega' = \omega - \omega_{21}$ is the angular frequency of the Raman scattered radiation. The matrix element $\langle p \rangle_{n1}$ associated with the momentum operator between the np and the $1s$ states is given by

$$\langle p \rangle_{n1} = \int_0^{\infty} R_{n1}(r) \left[\frac{d}{dr} R_{10}(r) \right] r^2 dr = \left[\frac{2^6 n^3 (n-1)^{2n-3}}{(n+1)^{2n+3}} \right]^{1/2}. \quad (23)$$

Here, an atomic unit system is adopted and the reality of the radial wavefunctions is noted.

The matrix element $\langle p \rangle_{n2}$ corresponds to the transition between the np and $2s$ states, which is explicitly given by

$$\langle p \rangle_{n2} = \left[\frac{2^{11} n^3 (n^2 - 1)(n - 2)^{2n-4}}{(n + 2)^{2n+4}} \right]^{1/2}. \quad (24)$$

The contribution from the continuum $n'p$ states is obtained by considering the matrix elements of the momentum operator given by

$$\begin{aligned} \langle p \rangle_{n'1} &= \left[\frac{2^6 n'^3 e^{-4n' \tan^{-1} \frac{1}{n'}}}{(n'^2 + 1)^3 (1 - e^{-2\pi n'})} \right]^{1/2} \\ \langle p \rangle_{n'2} &= \left[\frac{2^{11} n'^3 (n'^2 + 1) e^{-4n' \tan^{-1} \frac{2}{n'}}}{(n'^2 + 4)^4 (1 - e^{-2\pi n'})} \right]^{1/2}. \end{aligned} \quad (25)$$

Due to the vanishing matrix element $\langle p \rangle_{n2}$ for $n = 2$, the sum in Eq. (22) begins from $n = 3$ for the bound np states, which implies that the $2p$ state does not contribute to the cross section for Raman scattering around $\text{Ly}\beta$. This is decisively important to the behavior of the cross section, as we discuss later in more detail.

The terms involving angular frequencies can be rearranged using the following relation

$$\begin{aligned} \frac{\omega'}{\omega} &= \frac{\omega_{31} - \omega_{21} + \Delta\omega}{\omega_{31} + \Delta\omega} \\ &= \frac{\omega_{32}}{\omega_{31}} - \frac{\omega_{21}}{\omega_{31}} \sum_{k=1}^{\infty} \left(\frac{-\Delta\omega}{\omega_{31}} \right)^k, \end{aligned} \quad (26)$$

where $\omega_{32} = \omega_{31} - \omega_{21}$ is the angular frequency for $\text{H}\alpha$. Use is also made of the following relations

$$\begin{aligned} \frac{1}{\omega_{n1} - \omega} &= \frac{1}{\omega_{31}} \sum_{k=0}^{\infty} \left(\frac{\Delta\omega}{\omega_{31}} \right)^k \left(\frac{\omega_{31}}{\omega_{n1} - \omega_{31}} \right)^{k+1} \quad \text{for } n \geq 4 \\ \frac{1}{\omega_{n1} + \omega'} &= -\frac{1}{\omega_{31}} \sum_{k=0}^{\infty} \left(\frac{\Delta\omega}{\omega_{31}} \right)^k \left(\frac{-\omega_{31}}{\omega_{n1} + \omega_{31} - \omega_{21}} \right)^{k+1}. \end{aligned} \quad (27)$$

The Kramers-Heisenberg formula for Raman scattering near $\text{Ly}\beta$ can be expanded in frequency space as follows

$$\sigma^{Ram}(\omega) = \sigma_T \left(\frac{\omega_{31}}{\Delta\omega} \right)^2 \left(\frac{\omega'}{\omega} \right) \left| C_0 + C_1(\Delta\omega/\omega_{31}) + C_2(\Delta\omega/\omega_{31})^2 + \dots \right|^2, \quad (28)$$

where the coefficients C_k are given by

$$\begin{aligned} C_0 &= -\frac{\langle p \rangle_{32} \langle p \rangle_{31}}{3\omega_{31}} = -\frac{1}{2} \left(\frac{\omega_{32}}{\omega_{31}} \right)^{1/2} (f_{13} f_{2s,3p})^{1/2} \\ &= -3^4 \cdot 2^{1/2} \cdot 5^{-5} = -0.03666 \\ C_1 &= \frac{\langle p \rangle_{32} \langle p \rangle_{31}}{3(2\omega_{31} - \omega_{21})} + \frac{1}{3} \sum_{n \geq 4} \langle p \rangle_{n2} \langle p \rangle_{n1} \left(\frac{1}{\omega_{n1} - \omega_{31}} + \frac{1}{\omega_{n1} + \omega_{31} - \omega_{21}} \right) \\ &+ \frac{1}{3} \int_0^{\infty} dn' \langle p \rangle_{n'2} \langle p \rangle_{n'1} \left(\frac{1}{\omega_{n'1} - \omega_{31}} + \frac{1}{\omega_{n'1} + \omega_{31} - \omega_{21}} \right) = 1.018 \end{aligned} \quad (29)$$

and

$$\begin{aligned} C_k &= \sum_{n \geq 4} \frac{\langle p \rangle_{n2} \langle p \rangle_{n1}}{3\omega_{31}} \left[\left(\frac{\omega_{31}}{\omega_{n1} - \omega_{31}} \right)^k - \left(\frac{-\omega_{31}}{\omega_{n1} + \omega_{31} - \omega_{21}} \right)^k \right] \\ &+ \int_0^{\infty} dn' \frac{\langle p \rangle_{n'2} \langle p \rangle_{n'1}}{3\omega_{31}} \left[\left(\frac{\omega_{31}}{\omega_{n'1} - \omega_{31}} \right)^k - \left(\frac{-\omega_{31}}{\omega_{n'1} + \omega_{31} - \omega_{21}} \right)^k \right], \end{aligned} \quad (30)$$

for $k \geq 2$. Here, $f_{2s,3p} = \frac{2}{3}\omega_{32}^{-1}[\langle p \rangle_{32}]^2 = 0.4349$ is the oscillator strength between the $2s$ and $3p$ states (e.g. Bethe & Salpeter 1967).

Therefore, in frequency space the Raman scattering cross section is written as

$$\begin{aligned} \sigma^{Ram}(\omega) &= \sigma_T \left(\frac{\omega_{31}}{\Delta\omega_2} \right)^2 \frac{\omega_{32}}{\omega_{31}} |C_0|^2 \left[1 + \left(\frac{\omega_{21}}{\omega_{31}} + \frac{2C_1\omega_{32}}{C_0\omega_{31}} \right) \left(\frac{\Delta\omega_2}{\omega_{31}} \right) + \dots \right] \\ &= \sigma_T \left(\frac{\omega_{31}}{\Delta\omega_2} \right)^2 \frac{\omega_{32}}{\omega_{31}} |C_0|^2 \left[1 - 7.832 \left(\frac{\Delta\omega_2}{\omega_{31}} \right) + \dots \right]. \end{aligned} \quad (31)$$

In wavelength space, we obtain

$$\begin{aligned}
\sigma^{Ram}(\lambda) &\simeq \sigma_T \left(\frac{\lambda_\beta}{\Delta\lambda_2} \right)^2 \frac{5}{32} |C_0|^2 \left[1 + \left(-\frac{17}{5} - 2c_1 \right) \left(\frac{\Delta\lambda_2}{\lambda_\beta} \right) \right. \\
&\quad + \left(c_1^2 + \frac{44}{5}c_1 - \frac{49}{5} + 2c_2 \right) \left(\frac{\Delta\lambda_2}{\lambda_\beta} \right)^2 \\
&\quad \left. + \left(-2c_3 - 2c_1c_2 - \frac{27}{5}(c_1^2 - 2c_1 + 1 + 2c_2) \right) \left(\frac{\Delta\lambda_2}{\lambda_\beta} \right)^3 + \dots \right] \\
&= \sigma_T \left(\frac{\lambda_\beta}{\Delta\lambda_2} \right)^2 \frac{5}{32} |C_0|^2 [1 + 5.223 \times 10^1 (\Delta\lambda_2/\lambda_\beta) \\
&\quad + 9.103 \times 10^2 (\Delta\lambda_2/\lambda_\beta)^2 - 8.267 \times 10^3 (\Delta\lambda_2/\lambda_\beta)^3 + \dots], \tag{32}
\end{aligned}$$

where the lower case coefficients c_i are defined by $c_i = C_i/C_0$. The numerical values of these coefficients up to c_5 are shown in Table 1.

Unlike the case for Rayleigh scattering near $\text{Ly}\beta$, the Raman scattering cross section shows redward asymmetry with respect to the $\text{Ly}\beta$ center. This result can be traced to the fact that no contribution is made from the $2p$ state, which played a dominant role in the case of Rayleigh scattering near $\text{Ly}\beta$. In the absence of the $2p$ contribution, all the perturbing p states are more energetic than $\text{Ly}\beta$. This situation is exactly the same as the Rayleigh scattering around $\text{Ly}\alpha$ resulting in redward asymmetry.

The ratio $r_b(\lambda)$ of the cross sections for Raman scattering to Rayleigh scattering in the vicinity of $\text{Ly}\beta$ is given by

$$r_b(\lambda) = \frac{\sigma^{Ram}(\lambda)}{\sigma^{Ray}(\lambda)} = R_0 + R_1 \left(\frac{\Delta\lambda_2}{\lambda_\beta} \right) + R_2 \left(\frac{\Delta\lambda_2}{\lambda_\beta} \right)^2 + \dots \tag{33}$$

where the first three coefficients are explicitly $R_0 = (5|C_0|^2/32)/(f_{13}/2)^2 = 2^{18}5^{-9} = 0.1342$, $R_1 = 11.26$ and $R_2 = 535.9$. This result shows discrepancy with that provided by Yoo, Bak & Lee (2002), in which there is an error in their numerical calculation of the coefficients A_3 and A_4 . The leading term can also be expressed as $R_0 = (f_{2s,3p}/f_{13})(\omega_{32}/\omega_{31})^2 = 0.1342$, which implies that the branching ratio is determined by a combination of the oscillator strength and the phase space volume factor represented by ω^2 . It is seen that the dominant contribution is made by the phase space volume available to scattered radiation.

In Fig. 1, we show the branching ratio $r_b(\lambda)$ in the neighborhood of $\text{Ly}\beta$. The solid line shows the result from a direct numerical computation of the Kramers-Heisenberg formula. The dotted line shows the linear fit and the dot-dashed line shows the second order fit using Eq. (33). Because the coefficient R_2 is large, the nonlinearity of $r_b(\lambda)$ is quite conspicuous in the figure. This behavior leads to a redward shift in broad $\text{H}\alpha$ wings observed in young

planetary nebulae and symbiotic stars which are also attributed to Raman scattering of Ly β (Jung & Lee 2004).

2.4. Total scattering cross section around Ly β

In this subsection, we combine the results of previous subsections to provide the expansion of the total scattering cross section around Ly β . The total scattering cross section around Ly β is the sum of Eq. (20) and Eq. (31), which is, to the first order of $\Delta\omega_2/\omega_{31}$, given by

$$\sigma_{tot}(\omega) \simeq \sigma_{\beta} \left(\frac{\omega_{31}}{\Delta\omega_2} \right)^2 \left[1 + 31.37 \left(\frac{\Delta\omega_2}{\omega_{31}} \right) \right]. \quad (34)$$

Here, we introduce another parameter σ_{β} defined by

$$\sigma_{\beta} = \sigma_T (f_{13}/2)^2 [1 + 0.1342] = 1.180 \times 10^{-27} \text{ cm}^2. \quad (35)$$

In wavelength space, we may combine Eq. (21) and Eq. (32) to express the total scattering cross section around Ly β as

$$\sigma_{tot}(\lambda) \simeq \sigma_{\beta} \left(\frac{\lambda_{\beta}}{\Delta\lambda_2} \right)^2 \left[1 - 24.63 \left(\frac{\Delta\lambda_2}{\lambda_{\beta}} \right) \right]. \quad (36)$$

From this result, it is seen that the Ly β absorption profiles tend to shift blueward of the Ly β line center. In Fig. 2, we show the total scattering cross section obtained from a numerical evaluation of the Kramers-Heisenberg formula around Ly α and Ly β in wavelength space. The vertical axis shows the logarithm to the base 10 of $\sigma(\lambda)$ in units of cm^2 .

In order to take a clear view of the asymmetry of the scattering cross section we plot the same quantities in Fig 3 as a function of the absolute value of the wavelength deviation. The cross sections redward of Ly α and Ly β are shown with solid lines in the upper panel and lower panel, respectively. The dotted lines show the cross sections blueward of Ly α and Ly β . The dotted lines are mirror images of the curves blueward of Ly α and Ly β shown in Fig. 2. In Fig. 3, we see that red Ly α photons have larger scattering cross section than blue counterparts and that the opposite is the case for Ly β .

In Fig. 4, we show the transmission coefficient $t(\lambda, N_{HI})$ defined by

$$t(\lambda, N_{HI}) \equiv 1 - \exp[-\sigma(\lambda)N_{HI}] \quad (37)$$

for various neutral hydrogen column densities. The upper panel is for Ly α and the lower panel is for Ly β . The solid line shows the result for $N_{HI} = 10^{20} \text{ cm}^{-2}$, the dotted line for

$N_{HI} = 10^{21} \text{ cm}^{-2}$, and the dashed line for $N_{HI} = 5 \times 10^{21} \text{ cm}^{-2}$. In the case of $N_{HI} = 5 \times 10^{21} \text{ cm}^{-2}$, the asymmetry is quite noticeable in the scale shown in the figure.

3. Asymmetry in the Absorption Profiles of Ly α and Ly β

3.1. Absorption center shift

In this subsection, we investigate the shift of the absorption line center near Ly α and Ly β as a function of the neutral hydrogen column density. Denoting by λ_c the line center wavelength of Ly α or Ly β , the scattering cross section is approximated to the first order of dimensionless wavelength deviation from line center $x = \Delta\lambda/\lambda_c$ by a function

$$f(x) = \frac{1}{x^2} + \frac{a}{x}. \quad (38)$$

The equation $f(x) = k > 0$ has two solutions x_1, x_2 , of which the mean is $x_m = a/(2k)$. This implies that the absorption center can be meaningfully defined when we fix the value of cross section. The sign of the coefficient a determines the direction of asymmetry, where a positive a results in a red asymmetry.

Given a value of the H I column density N_{HI} we define the mean wavelength λ_{m1}^α of the two wavelengths $\lambda_{1,2}$ at which $\tau(\lambda_1) = \tau(\lambda_2) = \sigma(\lambda)N_{HI} = 1$ around Ly α and in a similar way we define λ_{m1}^β for Ly β . We also introduce λ_{m2}^α and λ_{m2}^β as the mean value of the two wavelengths $\lambda'_{1,2}$ where we have $\tau(\lambda'_1) = \tau(\lambda'_2) = 0.5$ around Ly α and Ly β , respectively. Corresponding to these wavelengths λ_{m1} , we define the velocity shift ΔV_1 by the relation

$$\Delta V_1^\alpha \equiv c(\lambda_{m1}^\alpha - \lambda_\alpha)/\lambda_\alpha \quad (39)$$

for Ly α and in a similar way ΔV_1^β is defined for Ly β . Here, c is the speed of light.

In Table 2, we show the values of λ_{m1}^α and λ_{m2}^α for various neutral hydrogen column densities. Also in Table 3 we show the quantities corresponding to the Ly β transitions. At $N_{HI} = 10^{21} \text{ cm}^{-2}$ we obtain a redward center shift in the amount of $\Delta\lambda = +16 \text{ km s}^{-1}$ for Ly α and a blueward shift of $\Delta\lambda = -3.9 \text{ km s}^{-1}$ for Ly β .

In Fig. 5, we show ΔV_1^α and ΔV_2^α as a function of N_{HI} in the cases of Ly α (upper panel) and ΔV_1^β and ΔV_2^β for Ly β (lower panel). The dotted line shows a fit to the data, which implies that both $\Delta V_1^{\alpha,\beta}$ and $\Delta V_2^{\alpha,\beta}$ are proportional to N_{HI} . The linear fit shown by the dotted line for Ly α in the figure is given by

$$\Delta V_1^\alpha \simeq 1.6 \left[\frac{N_{HI}}{10^{20} \text{ cm}^{-2}} \right] \text{ km s}^{-1}, \quad (40)$$

and similarly for Ly β it is given by

$$\Delta V_1^\beta \simeq -0.39 \left[\frac{N_{HI}}{10^{20} \text{ cm}^{-2}} \right] \text{ km s}^{-1}. \quad (41)$$

3.2. Profile fitting by shifting the Lorentzian

Another way of quantifying the asymmetry is provided by fitting the absorption profiles. In this subsection, we compare the transmission coefficient $t(\lambda, N_{HI})$ derived from the Kramers-Heisenberg formula with that obtained from the Lorentzian shifted by a finite amount. For simplicity, we fix the H I column density $N_{HI} = 5 \times 10^{21} \text{ cm}^{-2}$. This procedure may illustrate an error estimate in determining the redshift of a DLA system with $N_{HI} = 5 \times 10^{21} \text{ cm}^{-2}$.

In Fig. 6 we show the result for Ly α . The solid line in each panel shows the transmission coefficient obtained from the Kramers-Heisenberg formula. The dotted line in the top panel shows the transmission coefficient from the Lorentzian function, which provides an excellent fit near the line center. However, a considerable deviation in the wing part is quite noticeable. With the dotted line in the bottom panel, we show the quantities obtained by shifting the Lorentzian redward by an amount of $+0.8 \text{ \AA}$. Improvement of the fitting in wing parts is achieved only at the expense of a poor approximation near the line center. In the middle panel, we show the Lorentzian shifted by $+0.4 \text{ \AA}$, in which the quality of the fit is compromised between the previous two cases.

In the analysis by Lee (2003) the optimal wavelength shift was proposed by $+0.2 \text{ \AA}$, which is smaller than $+0.4 \text{ \AA}$ suggested in this work. This discrepancy is due to the fact that the fitting procedure in Lee (2003) was confined to a rather narrow interval of $|\Delta\lambda| < 34 \text{ \AA}$ excluding extreme wing parts. The procedure of fitting a DLA profile using the shifted Lorentzian tends to overestimate the line center wavelength of Ly α leading to corresponding overestimate of the redshift of the DLA. We note that Lee (2003) made a mistake in pointing out that the redshift would be '*underestimated*', which should be corrected to be '*overestimated*'.

A similar analysis corresponding to Ly β is shown in Fig. 7 for the same neutral hydrogen column density $N_{HI} = 5 \times 10^{21} \text{ cm}^{-2}$. In the figure, the dotted line in each panel shows the transmission coefficient from the Lorentzian function (top panel) and shifted Lorentzian functions (middle and bottom panels), whereas the solid line shows the exact transmission coefficient computed from the Kramers-Heisenberg formula. The amount of wavelength shift blueward of Ly β is $\Delta\lambda = -0.1 \text{ \AA}$ and -0.2 \AA for the middle and bottom panels, respectively. As in the case of Ly α illustrated in Fig. 6, the unshifted Lorentzian gives an excellent fit to

the core part of the absorption profile whereas the bottom panel shows an improved fit to the wing parts with the loss of fitting quality at the core part.

In Fig. 8, we present the transmission coefficients using the Kramers-Heisenberg formula and the Lorentzian functions around Ly α and Ly β in the wavelength interval between 980 Å and 1400 Å for a very thick H I medium with $N_{HI} = 5 \times 10^{22} \text{ cm}^{-2}$. This kind of an extreme neutral hydrogen column density has been found toward the gamma ray burst GRB080607 (e.g. Prochaska et al. 2009). For comparison, we show the transmission coefficients obtained from the Lorentzian around Ly α and Ly β by the dotted line and the dashed line, respectively. In this highly thick medium, the deviation from the Lorentzian is quite severe due to the contribution from higher order terms, which prevents one from obtaining satisfactory results by fitting the absorption profiles by a Voigt or equivalently a Lorentzian function.

In particular, in the wavelength range shown in Fig. 8, the local peak transmission is found at $\lambda_p = 1062 \text{ Å}$, for which $t(\lambda, N_{HI} = 5 \times 10^{22} \text{ cm}^{-2}) = 0.0144$. However, the sum of two Lorentzian functions around Ly α and Ly β admits a local maximum at $\lambda = 1070 \text{ Å}$. This shows the inadequacy of using a Voigt function for fitting analyses in extended wing parts in the case of very high column density systems. Furthermore, at this high N_{HI} , the blue wing region of Ly α overlaps with that of the red Ly β wing, for which full quantum mechanical formula should be invoked for an accurate analysis.

4. Summary and Discussion

The Kramers-Heisenberg formula is expanded around Ly α and Ly β in order to investigate the asymmetric deviation of the scattering cross section. A redward asymmetry is seen around Ly α and a blueward asymmetry is found around Ly β . For red Ly α photons the perturbing transitions from $(n + n')p$ states ($n \neq 2$) provide a positive contribution to the scattering cross section because they are in the same side as the $2p$ state in the energy space, resulting in red asymmetry. In the case of Ly β , Rayleigh scattering contributes more than Raman scattering by a factor 6.452. Raman scattering around Ly β exhibits a red asymmetry like Ly α because all the perturbing transitions lie higher than the main transition. However, for Rayleigh scattering around Ly β , the transition from $2p$ state is the dominant perturbing transition which is less energetic than Ly β . This leads to a blue asymmetry in $\sigma(\lambda)$ around Ly β . In an attempt to quantify these asymmetries we compute the mean wavelengths for which the scattering optical depth becomes a unity or one half for various values of H I column density N_{HI} . Also we fitted the transmission coefficients for given N_{HI} by shifting the Lorentzian function.

Peebles (1993) introduced the formula for resonance scattering cross section around Ly α

$$\sigma_P(\omega) = \frac{3\lambda_\alpha^2\Lambda^2}{8\pi} \frac{(\omega/\omega_\alpha)^4}{(\omega - \omega_\alpha)^2 + (\Lambda^2/4)(\omega/\omega_\alpha)^6}, \quad (42)$$

which is often used in fitting wing profiles of Ly α (e.g. Miralda-Escude 1998). In particular, the red damping wing of Ly α is essential to probe the partially neutral intergalactic medium expected around the end of cosmic reionization (Gunn & Peterson 1965, Scheuer 1965, Mortlock et al. 2011). Neglecting the damping term in the denominator, this expression yields an expansion in frequency space

$$\sigma_P(\omega) \simeq \sigma_\alpha \left(\frac{\omega_\alpha}{\Delta\omega} \right)^2 \left[1 + 4 \left(\frac{\Delta\omega}{\omega_\alpha} \right) \right]. \quad (43)$$

In this expression, the coefficient of the first order term is 4, which differs significantly from the correct value of -1.792 . According to this formula, the scattering cross section is larger in the blue part of Ly α than in the red part, which is incorrect. The discrepancy in the expansion may be traced to the approximation adopted in the derivation of Eq. (42), where the hydrogen atom is effectively treated as a two level system.

The Lorentzian or Voigt profile matches the Kramers-Heisenberg profile excellently only in the core part. Therefore, the redshift will be measured reliably when the profile fitting is more weighted toward deeply absorbed core part than far wing parts. With the accurate determination of the redshift and column density of the DLA, one may obtain reliable transmission coefficients using the Kramers-Heisenberg formula or its first order approximation given in Eq. (10) and Eq. (36).

In an analysis of a quasar spectrum, it is highly difficult to obtain the accurate continuum level due to intervening Ly α forest systems. Securing the quasar continuum level around the damped Ly α center with high precision is critical to verify the asymmetry presented in this work. With the advent of extremely large telescopes in the near future equipped with a high resolution spectrometer the accurate atomic physics will shed light on the physical conditions of neutral hydrogen reservoir in the early universe.

The author is very grateful to the anonymous referee whose comments greatly improved the presentation of this paper. This research was supported by the Basic Science Research Program through the National Research Foundation of Korea (NRF) funded by the Ministry of Education, Science and Technology (2011-0027069).

A. Angle Averaged Cross Section

We show a detailed angular integration of the matrix element that constitute the Kramers-Heisenberg formula. Because of the selection rule of the electric dipole interaction, the relevant states are np and $1s$ state in the case of Rayleigh scattering. In the case of Raman scattering relevant to the interaction around $Ly\beta$, $2s$ state is also involved. However, as long as the angular and polarization average is concerned, the same calculation is performed.

A typical matrix element to be summed in the Kramers-Heisenberg formula is

$$M(\hat{\mathbf{e}}^{(\alpha)}, \hat{\mathbf{e}}^{(\alpha')}, 1s, I) = (\mathbf{r} \cdot \hat{\mathbf{e}}^{(\alpha')})_{1s, I} (\mathbf{r} \cdot \hat{\mathbf{e}}^{(\alpha)})_{I, 1s}, \quad (\text{A1})$$

where I denotes an intermediate state. In particular, I can be written as $I = |np, m\rangle$, where m is the magnetic quantum number taking one of zero and ± 1 in the case of a p -state. The spherical harmonic functions with $l = 1$ are explicitly defined by

$$Y_1^1(\theta, \phi) = -\frac{1}{2}\sqrt{\frac{3}{2\pi}}\sin\theta e^{i\phi}, \quad Y_1^{-1}(\theta, \phi) = \frac{1}{2}\sqrt{\frac{3}{2\pi}}\sin\theta e^{-i\phi}, \quad Y_1^0(\theta, \phi) = \frac{1}{2}\sqrt{\frac{3}{\pi}}\cos\theta, \quad (\text{A2})$$

from which we may set

$$\frac{x}{r} = \sqrt{\frac{2\pi}{3}}(Y_1^{-1} - Y_1^1), \quad \frac{y}{r} = i\sqrt{\frac{2\pi}{3}}(Y_1^{-1} + Y_1^1), \quad \frac{z}{r} = 2\sqrt{\frac{\pi}{3}}Y_1^0. \quad (\text{A3})$$

Therefore given an intermediate state $I = |np, m\rangle$, we have

$$M(\hat{\mathbf{e}}^{(\alpha)}, \hat{\mathbf{e}}^{(\alpha')}, 1s, I) = \langle 1s | (xe_x^\alpha + ye_y^\alpha + ze_z^\alpha) | np, m \rangle \langle np, m | (xe_x^{\alpha'} + ye_y^{\alpha'} + ze_z^{\alpha'}) | 1s \rangle. \quad (\text{A4})$$

The wavefunction $|np, m\rangle$ is given by the product of the radial part $R_{n1}(r)$ and angular part Y_1^m , where as the $1s$ state is characterized by the radial part $R_{10}(r)$ multiplied by the trivial spherical harmonic $Y_0^0 = 1/\sqrt{4\pi}$. Therefore, we have

$$\begin{aligned} \langle 1s | x | np, m \rangle &= \langle 1s | r | np \rangle \int d\Omega Y_0^0 \left[\frac{x}{r} \right] Y_1^m \\ &= \langle 1s | r | np \rangle (4\pi)^{-1/2} \sqrt{\frac{2\pi}{3}} [\delta_{m,-1} - \delta_{m,1}] \\ &= \langle 1s | r | np \rangle \frac{1}{\sqrt{6}} [\delta_{m,-1} - \delta_{m,1}]. \end{aligned} \quad (\text{A5})$$

Here, $\delta_{m,n}$ is the Kronecker delta and $\langle 1s | r | np \rangle = \int_0^\infty R_{10}(r) r R_{n1}(r) r^2 dr$ is the radial expectation value between $1s$ and np state. In a similar way, for the operator y and z we

have

$$\begin{aligned}
 \langle 1s|y|np, m \rangle &= \langle 1s|r|np \rangle \frac{i}{\sqrt{6}} [\delta_{m,-1} + \delta_{m,1}] \\
 \langle 1s|z|np, m \rangle &= \langle 1s|r|np \rangle \frac{i}{\sqrt{3}} \delta_{m,0}.
 \end{aligned} \tag{A6}$$

From this we note that

$$\begin{aligned}
 M(\hat{\mathbf{e}}^{(\alpha)}, \hat{\mathbf{e}}^{(\alpha')}, 1s, I) &= |\langle 1s|r|np \rangle|^2 \left[\frac{1}{\sqrt{6}} (\delta_{m,-1} - \delta_{m,1}) e_x^\alpha + \frac{i}{\sqrt{6}} (\delta_{m,-1} + \delta_{m,1}) e_y^\alpha \right. \\
 &\quad \left. + \frac{1}{\sqrt{3}} \delta_{m,0} e_z^\alpha \right] \times \left[\frac{1}{\sqrt{6}} (\delta_{m,-1} - \delta_{m,1}) e_x^{\alpha'} \right. \\
 &\quad \left. + \frac{-i}{\sqrt{6}} (\delta_{m,-1} + \delta_{m,1}) e_y^{\alpha'} + \frac{1}{\sqrt{3}} \delta_{m,0} e_z^{\alpha'} \right] \\
 &= |\langle 1s|r|np \rangle|^2 \left[\frac{1}{6} \delta_{m,-1} (e_x^\alpha + i e_y^\alpha) (e_x^{\alpha'} - i e_y^{\alpha'}) \right. \\
 &\quad \left. + \frac{1}{6} \delta_{m,1} (-e_x^\alpha + i e_y^\alpha) (-e_x^{\alpha'} - i e_y^{\alpha'}) + \frac{1}{3} \delta_{m,0} e_z^\alpha e_z^{\alpha'} \right]
 \end{aligned} \tag{A7}$$

Given np states, we sum over substates with $m = \pm 1, 0$ to obtain

$$\sum_{m=\pm 1,0} M(\hat{\mathbf{e}}^{(\alpha)}, \hat{\mathbf{e}}^{(\alpha')}, 1s, I) = \frac{1}{3} |\langle 1s|r|np \rangle|^2 (\mathbf{e}^\alpha \cdot \mathbf{e}^{\alpha'}). \tag{A8}$$

As is well-known for Thomson scattering (e.g. pages 51 and 52 in Sakurai 1967), a numerical factor of $8\pi/3$ results from averaging over polarization states for both incoming and outgoing radiation.

REFERENCES

- Arrieta, A., Torres-Peimbert, S., 2003, *ApJS*, 147, 97
- Berestetskii, V.B., Lifshitz, E.M., & Pitaevskii, L.P., 1971, *Relativistic Quantum Mechanics*, Pergamon Press
- Bethe, H. A. & Salpeter, E. E. 1967, *Quantum Mechanics of One and Two Electron Atoms*, Academic Press Inc., New York
- Birriel, J., 2004, *ApJ*, 612, 1136
- Calura, F., Matteucci, F., Vladilo, G., 2003, *MNRAS*, 340, 59

- Curran, S. J., Webb, J. K., Murphy, M. T., Bandiera, R., Corbelli, E., Flambaum, V. V., 2002, *PASA*, 19, 455
- Gunn, J. E., Peterson, B. A., 1965, *ApJ*, 142, 1633
- Islaker, H., Nussbaumer, H., & Vogel, M., 1989, *A& A*, 219, 271
- Jung, Y.-C., Lee, H.-W., 2004, *MNRAS*, 350, 580
- Khare, P., vanden Berk, D., York, D. G., Lundgren, B., Kulkarni, V. P., 2012, *MNRAS*, 419, 1028
- Kim, J., Park, C., Rossi, G., Lee, S. M., Gott III, R., 2011, *Journal of the Korean Astronomical Society*, 44, 217
- Kulkarni, V. P., Meiring, J., Som, D., Péroux, C., York, D. G., Khare, P., Lauroesch, J. T., 2012, *ApJ*, 749, 176
- Lee, H. -W., 2000, *ApJ*, 541, L25
- Lee, H. -W., 2003, *ApJ*, 594, 637
- Lee, H. -W., 2012, *ApJ*, 750, 127
- Lee, H. -W., Lee, K. W., 1997, *MNRAS*, 287, 211
- Lee, H. -W., Jung, Y. -C., Song, I. -O., Ahn, S. -H., 2006, *ApJ*, 636, 1045
- Meiksin, A. A., 2009, *Reviews of Modern Physics*, 81, 2405
- Merzbacher, E. 1970, *Quantum Mechanics*, Wiley, New York
- Miralda-Escudé, J., 1998, *ApJ*, 501, 15
- Mortlock, D. J. et al. 2011, *Nature*, 474, 616
- Noterdaeme, P., Laursen, P., Petitjean, P., Vergani, S. D., Maureira, M. J., Ledoux, C., Fynbo, J. P. U., López, S., Srianand, R., 2012, *A& A*, 540, A63
- Nussbaumer, H., Schmid, H. M. & Vogel, M., 1989, *A&A*, 221, L27
- Peebles, P. J. E., 1993, *Principles of Physical Cosmology*, Princeton University Press, Princeton
- Prochaska, J. X., Herbert-Fort, S., Wolfe, A. M., 2005, *ApJ*, 635, 123

- Prochaska, J. X. et al., 2009, ApJ, 691, L127
- Rafelski, M., Wolfe, A. M., Prochaska, J. X., Neeleman, M., Medez, A. J., 2012, ApJ, 755, 89
- Rauch, M., 1998, ARA&A, 36, 267
- Rybicki, G. B., Lightman, A. P., 1979, Radiative Processes in Astrophysics, Wiley-Interscience, New York
- Sakurai, J. J., 1967, Advanced Quantum Mechanics, Addison-Wesley Publishing Company, Reading, Massachusetts
- Saslow, W. M., Mills, D. L. 1969, Physical Review, 187, 1025
- Scheuer, P. A. G. 1965, Nature, 207, 963
- Schmid, H. M. 1989, A& A, 211, L31
- Wolfe, A., Turnshek, D. A., Smith, H. E., Cohen, R. D., 1986, ApJS, 61, 249
- Wolfe, A., Gawiser, E., Prochaska, J. X., 2005, ARA&A, 43, 861
- Yoo, J. J., Bak, J.-Y., Lee, H.-W., 2002, MNRAS, 336, 467

This preprint was prepared with the AAS L^AT_EX macros v5.2.

Ly α	Ly β	Ly β (Raman)
$a_1 = -8.961 \times 10^{-1}$	$b_1 = 1.621 \times 10^1$	$c_1 = -2.776 \times 10^1$
$a_2 = -1.222 \times 10^1$	$b_2 = -4.299 \times 10^2$	$c_2 = -2.128 \times 10^2$
$a_3 = -5.252 \times 10^1$	$b_3 = -2.176 \times 10^3$	$c_3 = -3.231 \times 10^3$
$a_4 = -2.438 \times 10^2$	$b_4 = -6.005 \times 10^4$	$c_4 = -1.098 \times 10^5$
$a_5 = -1.210 \times 10^3$	$b_5 = -8.414 \times 10^5$	$c_5 = -4.032 \times 10^6$

Table 1: Expansion coefficients of Rayleigh scattering cross section around Ly α and Rayleigh and Raman scattering cross sections around Ly β .

$\log N_{HI}$	λ_{m1}^α (Å)	ΔV_1^α (km s ⁻¹)	λ_{m2}^α (Å)	ΔV_2^α (km s ⁻¹)
19.0	6.10E-04	0.151	1.34E-03	0.331
19.7	3.30E-03	0.813	6.47E-03	1.60
20.0	6.47E-03	1.60	1.32E-02	3.25
20.7	3.26E-02	8.04	6.51E-02	16.0
21.0	6.51E-02	16.0	1.30E-01	32.1
21.7	3.25E-01	80.2	6.51E-01	1.60E+02
22.0	6.51E-01	1.60E+02	1.31	3.20E+02
22.7	3.25	8.01E+02	6.48	1.60E+03

Table 2: Absorption center shifts around Ly α for various neutral hydrogen column densities.

$\log N_{HI}$	λ_{m1}^β (Å)	ΔV_1^β (km s ⁻¹)	λ_{m2}^β (Å)	ΔV_2^β (km s ⁻¹)
19.0	-1.22E-04	-0.03568	-2.44E-04	-0.07136
19.7	-7.32E-03	-0.214	-1.34E-03	-0.392
20.0	-1.34E-03	-0.392	-2.69E-02	-0.785
20.7	-6.59E-03	-1.93	-1.34E-02	-3.92
21.0	-1.34E-02	-3.92	-2.67E-02	-7.81
21.7	-6.64E-02	-19.4	-1.32E-01	-38.5
22.0	-1.32E-01	-38.5	-2.60E-01	-75.9
22.7	-6.22E-01	-1.82E+02	-1.16	-3.38E+02

Table 3: Absorption center shifts around Ly β for various neutral hydrogen column densities.

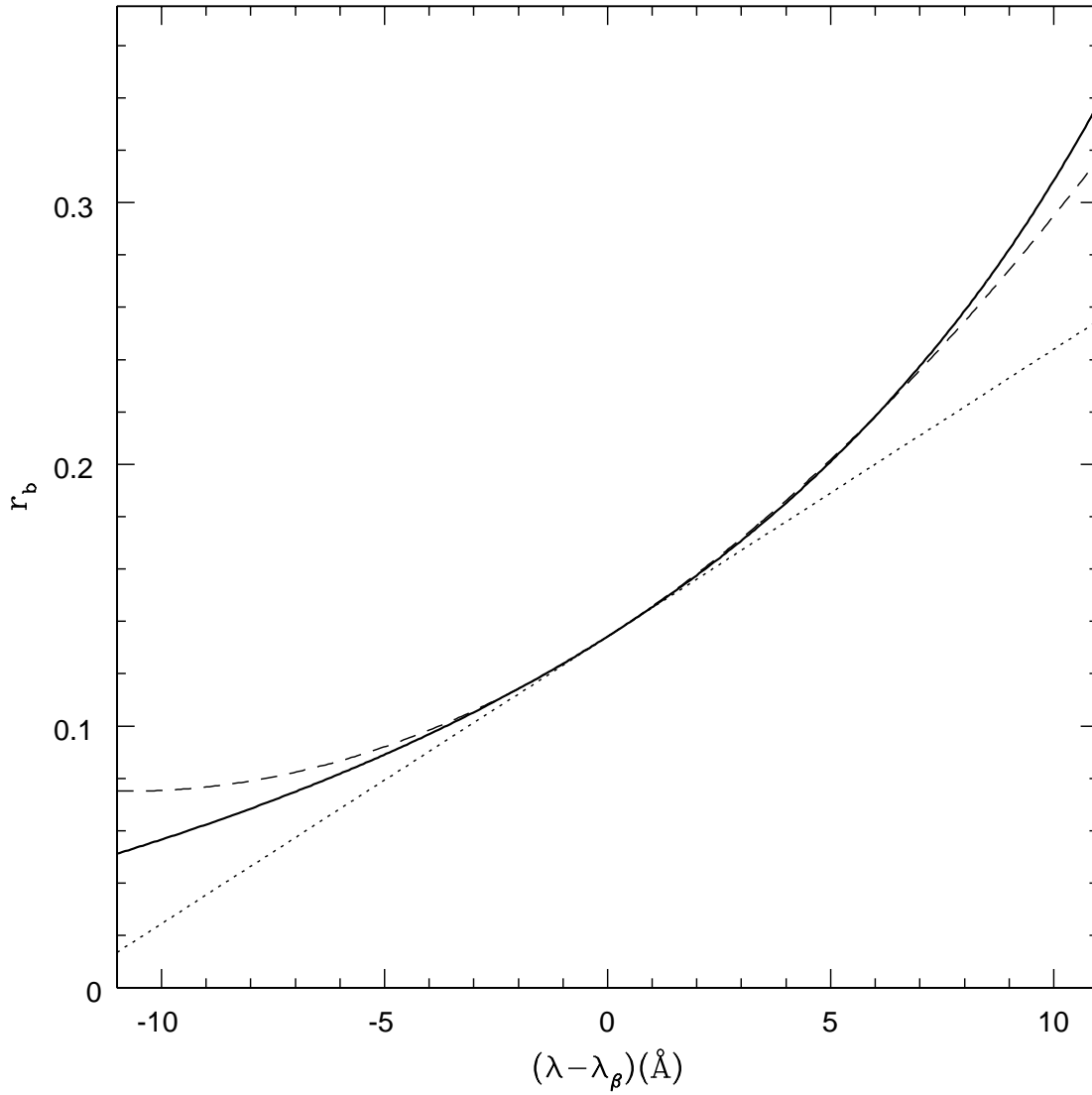


Fig. 1.— Ratio of cross sections of Raman scattering and Rayleigh scattering around $\text{Ly}\beta$. The solid line shows the result from the full numerical calculation of the Kramers-Heisenberg formula. The dotted line shows the linear fit and the dashed line shows the quadratic fit.

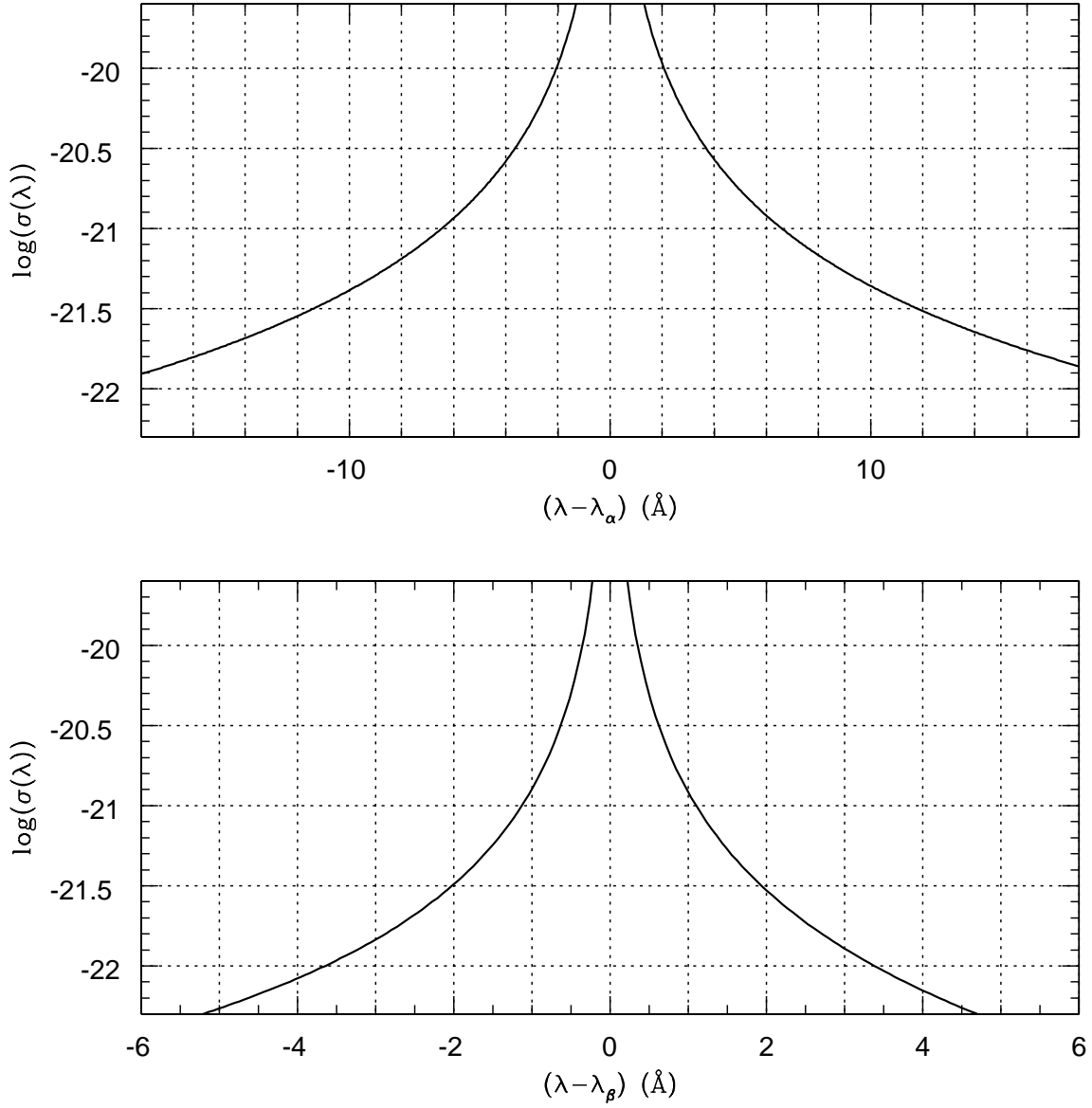


Fig. 2.— Scattering cross section around Ly α (upper panel) and Ly β (lower panel). The horizontal axis shows the wavelength difference from the line center and the vertical axis represents the logarithm of the cross section in units of cm^2 .

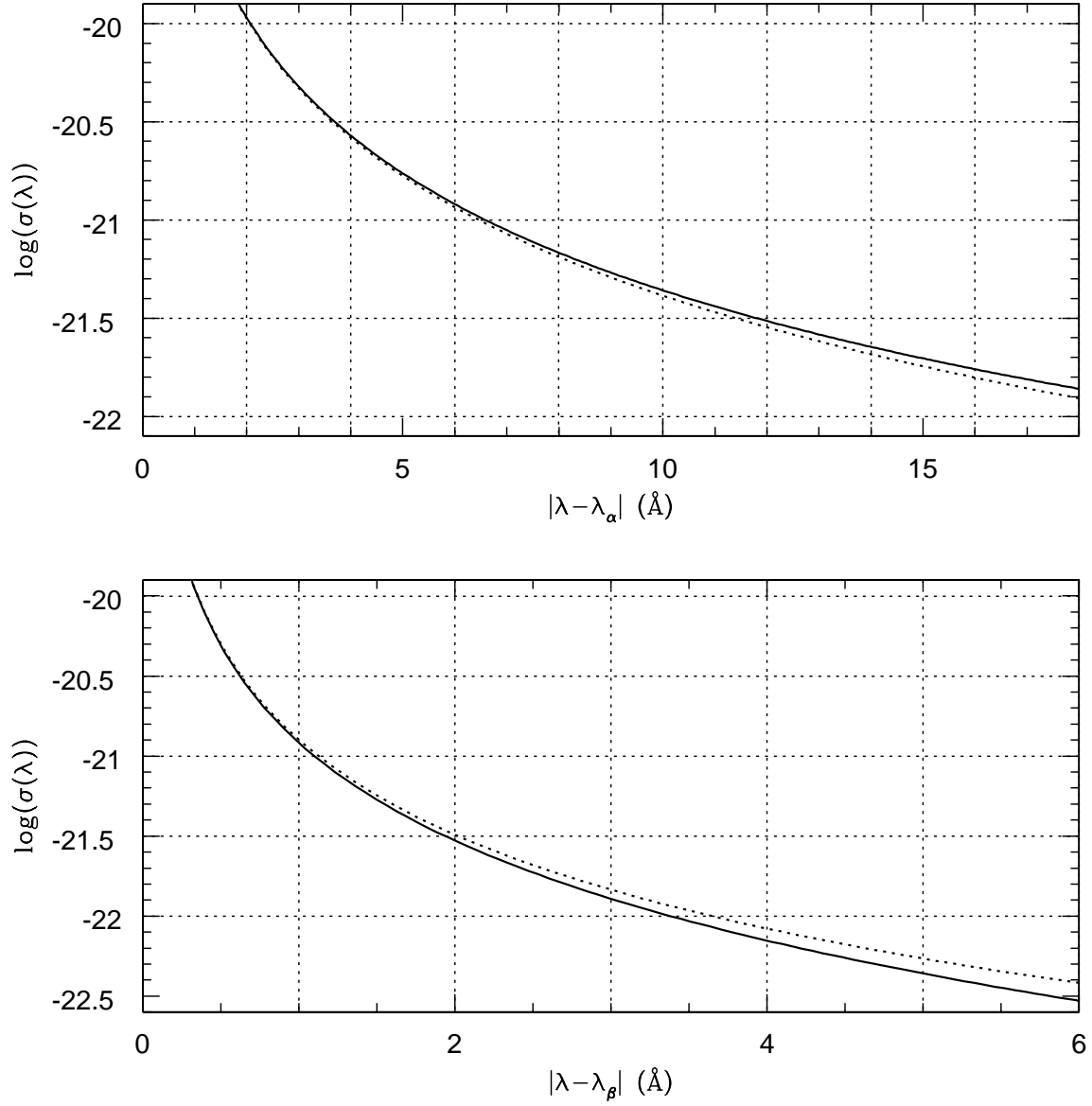


Fig. 3.— Scattering cross section around Ly α (upper panel) and Ly β (lower panel) as a function of the absolute value of the wavelength difference. The solid lines show the cross section redward of Ly α (upper panel) and Ly β (lower panel). The cross sections blueward of Ly α and Ly β are shown in dotted lines in the upper panel and lower panel, respectively.

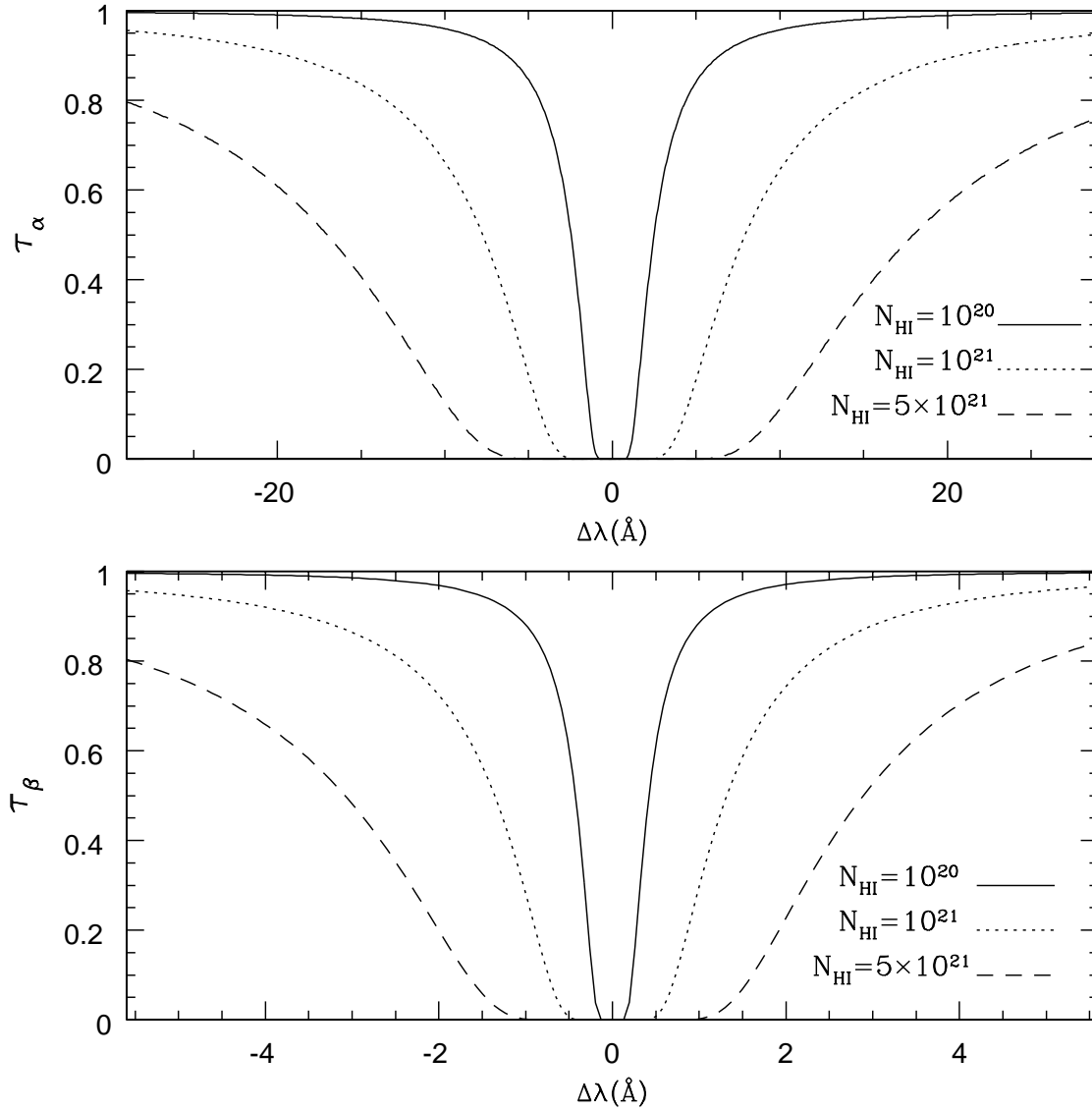


Fig. 4.— Absorption profiles around Ly α (upper panel) and Ly β (lower panel) for various neutral hydrogen column densities.

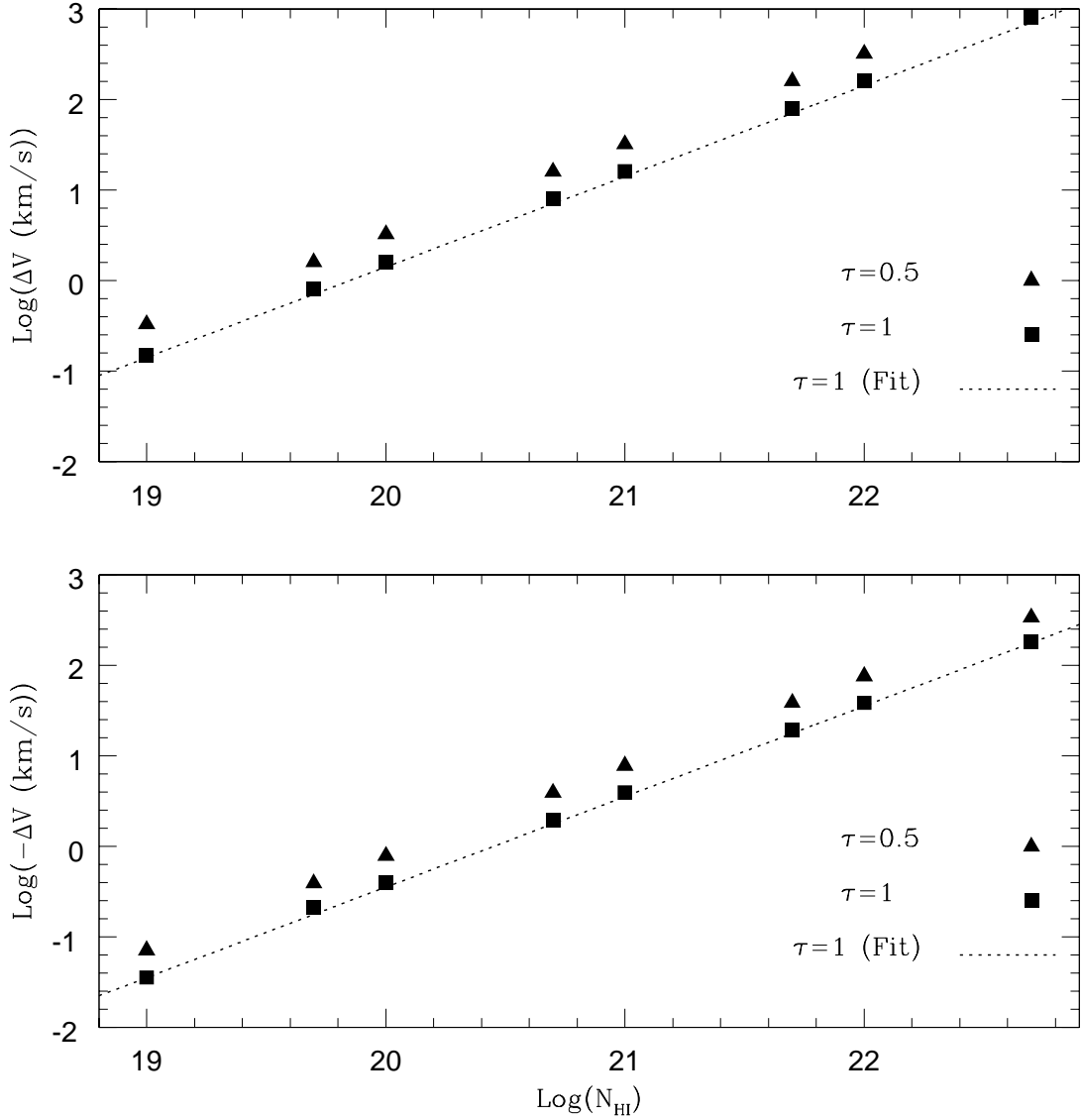


Fig. 5.— Center shift of the absorption profile around Ly α (upper panel) and around Ly β (lower panel). The horizontal axis shows the logarithm of the H I column density. The squares show the absorption center defined by the mean values of the wavelengths where $\tau(\lambda) = 1$. The triangles show the absorption center similarly defined by the condition $\tau(\lambda) = 0.5$.

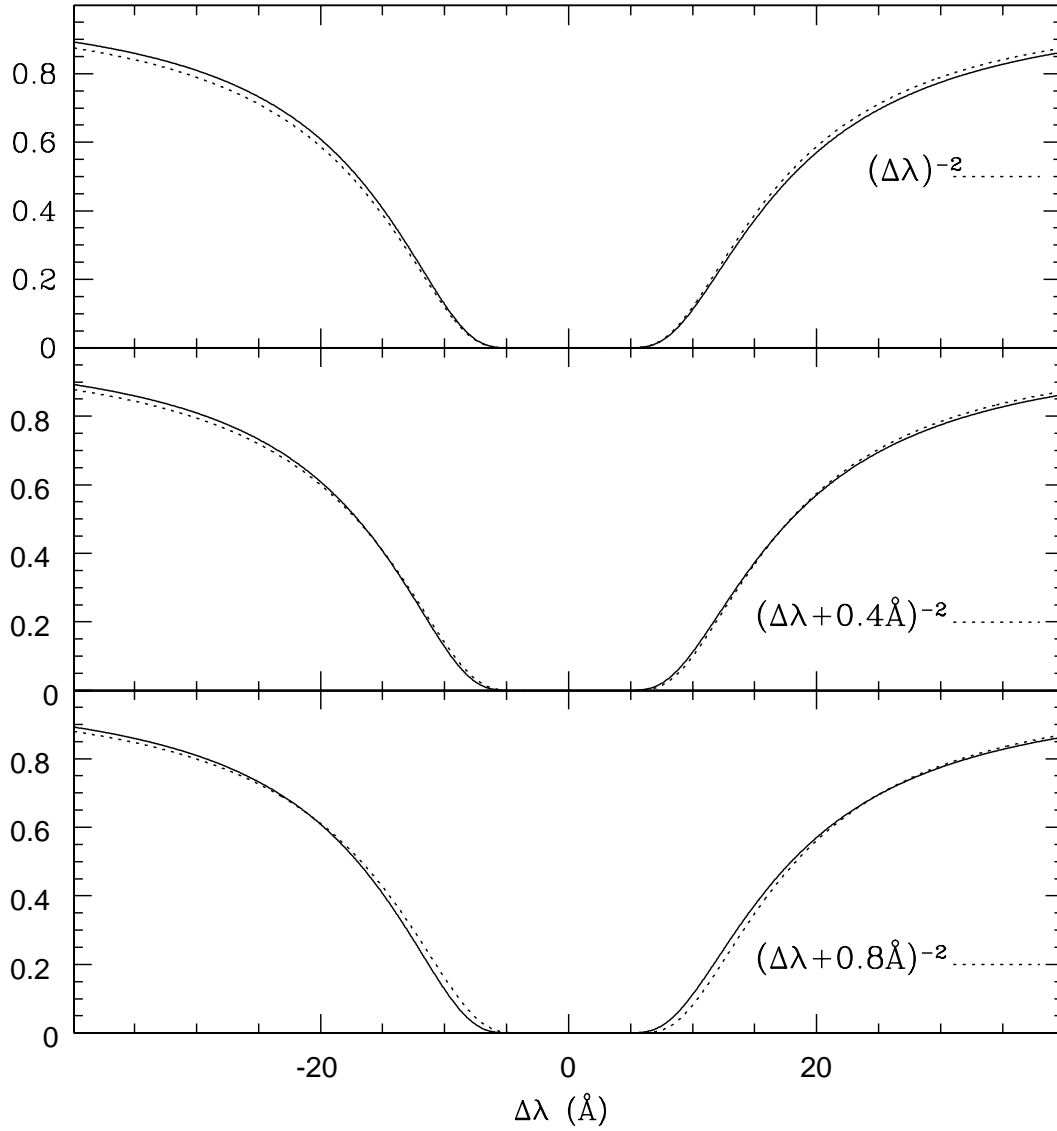


Fig. 6.— Fit to the absorption profile around Ly α using shifted Lorentzian functions. The solid line is the transmission probability for a neutral slab of hydrogen with $N_{HI} = 5 \times 10^{21} \text{ cm}^{-2}$.

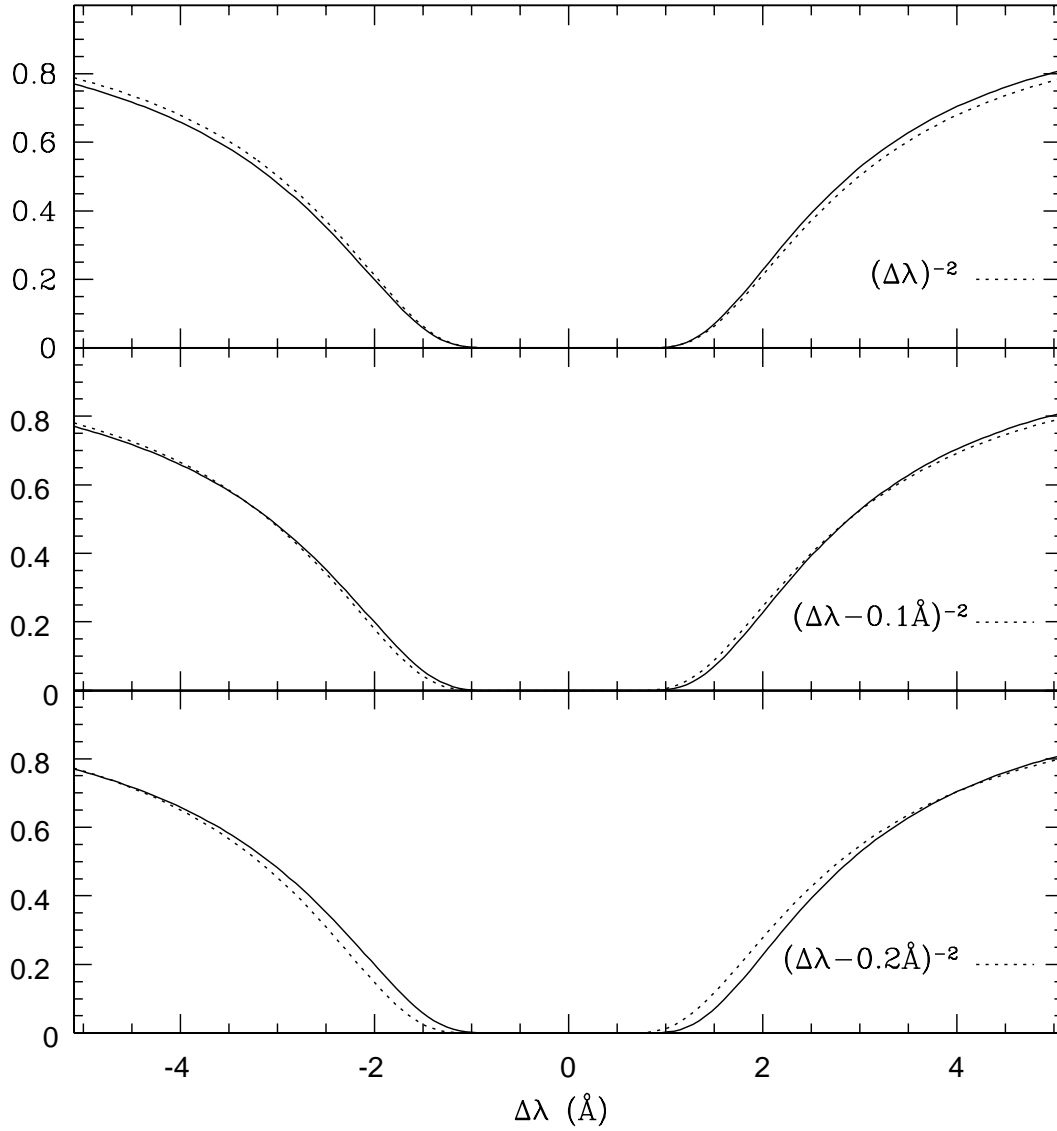


Fig. 7.— Fit to the absorption profile around $\text{Ly}\beta$ using shifted Lorentzian functions. The solid line is the transmission probability for a neutral slab of hydrogen with $N_{HI} = 5 \times 10^{21} \text{ cm}^{-2}$.

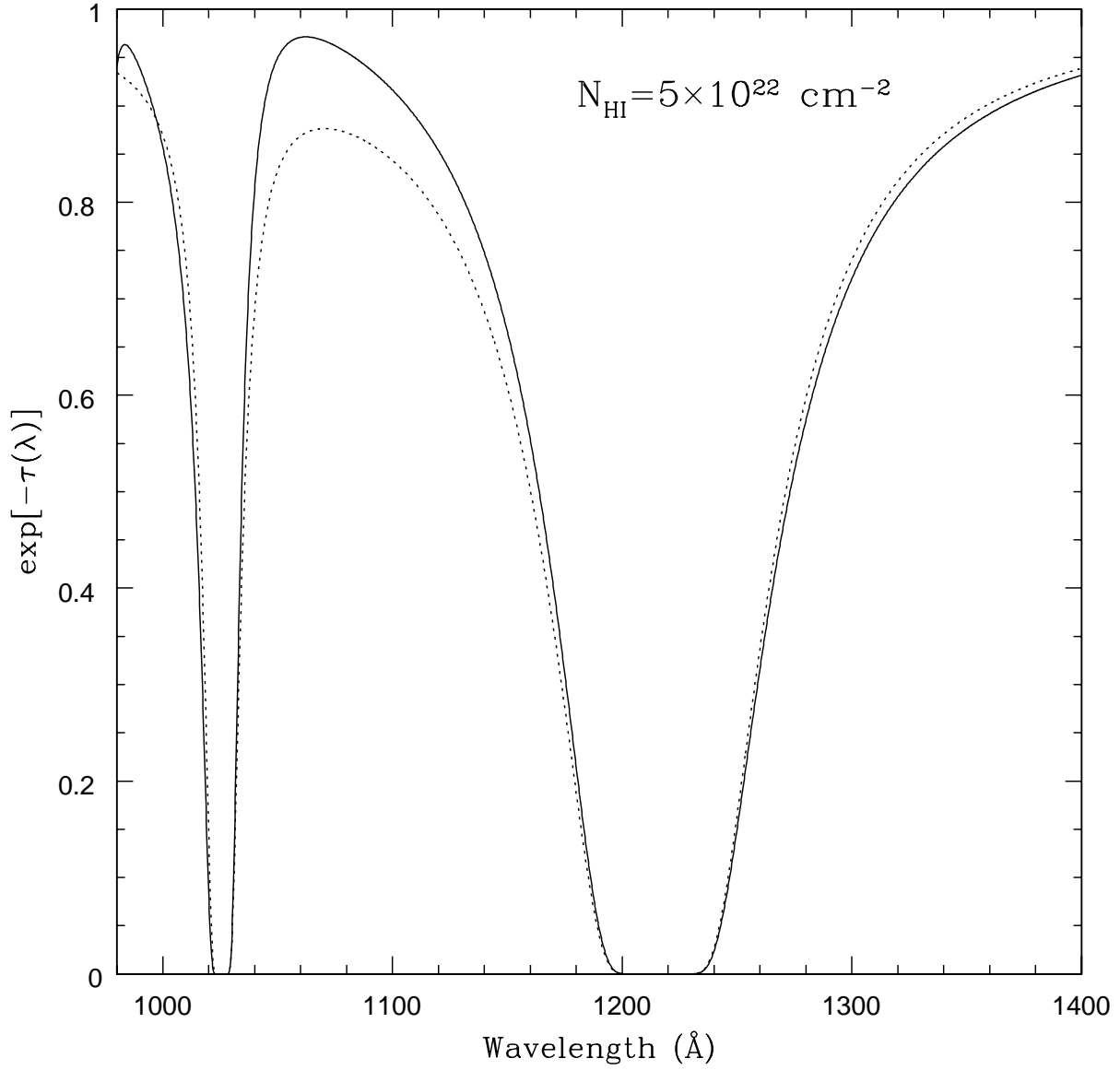


Fig. 8.— Absorption profile in the wavelength region between 980 \AA and 1400 \AA for a slab of a neutral hydrogen column density $N_{\text{HI}} = 5 \times 10^{22} \text{ cm}^{-2}$. The dotted line shows the transmission coefficient obtained from the sum of the two Lorentzian functions around Ly α and around Ly β .